Available online at www.sciencedirect.com
SCIENCE DIRECT®
Journal of Magnetic Resonance 158 (2002) 15–22
JMR Journal of Magnetic Resonance
www.academicpress.com

Condition for adiabatic passage in the earth's-field NMR technique

B.F. Melton* and V.L. Pollak

Department of Physics, The University of North Carolina at Charlotte, Charlotte, NC 28223, USA

Received 18 October 2001; revised 28 June 2002

Abstract

The equation of motion $d\mathbf{M}/dt = \gamma \mathbf{M} \times \mathbf{B}(t)$ is solved for the case $\mathbf{B}(t) = \mathbf{j}B_p(t) + \mathbf{k}B_e$. The field B_e is a small static field, typically the earth's field. The field $B_p(t)$ decays exponentially toward zero with time constant T. This decay is produced by an overdamped switching transient that occurs near the end of the rapid cutoff of the coil current used to polarize the sample. It is assumed that B_p is initially large compared to B_e, and that magnetization $\mathbf{M}$ is initially along the resultant field $\mathbf{B}$. Exact solutions are obtained numerically for several decay time constants of B_p, and the motion of $\mathbf{M}$ is depicted graphically. It is found that for adiabatic passage, the final cone angle β of the precession in field B_e is related to the decay time constant of B_p by $\beta = 2e^{-(\pi/2)\omega_e T}$. This is confirmed by measurements of the amplitudes of the ensuing free-precession signals for various decay rates of B_p. Near-perfect adiabatic passage (magnetization aligned within 2° of the earth's field) can be achieved for time constants $T \geqslant 2.6/\omega_e$. For the case of sudden passage, an approximate analytic solution is developed by linearizing the equation of motion in the laboratory frame of reference. For the adiabatic case, an approximate analytic solution is obtained by linearizing the equation of motion in a rotating frame of reference that follows the resultant field $\mathbf{B} = \mathbf{B}_p + \mathbf{B}_e$.

Keywords: Earth's field; NMR; Adiabatic passage; Sudden passage; Free precession

1. Introduction

The earth's-field NMR technique differs from standard techniques in that a single current-carrying coil suffices to polarize the sample, to manipulate the direction of the nuclear magnetization, and to detect the free-precession signal. In essence, the sample coil is oriented with its axis perpendicular to the earth's magnetic field, and a large current produces a buildup of the nuclear magnetization. After the current is cut off, this magnetization precesses about the earth's field, inducing an emf in the coil. The resulting signal is then amplified, displayed, and measured.

In the first paper of this series [1] we referenced a variety of applications of this technique. These include earth's-field magnetometry, research on spin relaxation in liquids and solutions, self-diffusion measurements, and well logging. Magnetic resonance imaging has also been shown to be possible using earth's-field NMR. In [1] we then analyzed the details of the motion of the magnetization $\mathbf{M}$ during *linear* cutoff of the polarizing field B_p and developed the relationship between the cutoff rate and the ensuing orientation of the magnetization. The cutoff rate can range from very fast (*sudden passage*), which leaves $\mathbf{M}$ precessing close to the plane perpendicular to the earth's field, to very slow (*adiabatic passage*), in which $\mathbf{M}$ remains more or less aligned along the *resultant* field during the cutoff.

From a practical point of view, however, it is essential that the analysis be carried out for a time dependence of B_p that can be achieved readily with electronic circuitry. The latter invariably involves not only the resistance and inductance of the coil, but also its stray capacitance. Accordingly, in a later paper [2] we analyzed the motion of $\mathbf{M}$ under the more readily attainable condition in which the B_p cutoff makes a transition from linear to damped oscillatory decay, with the initial oscillation amplitude large compared to the earth's field B_e. In this case the motion of $\mathbf{M}$ depends on the characteristics of the damped oscillation. We then showed that, by appropriate adjustment of the damping, it is possible to

* Corresponding author. Fax: 1-704-687-3160.
E-mail address: bfmelton@email.uncc.edu (B.F. Melton).

1090-7807/02/$ - see front matter © 2002 Elsevier Science (USA). All rights reserved.
PII: S1090-7807(02)00001-0

attain the condition of *idealized* sudden passage, which leaves the magnetization precessing precisely perpendicular to the earth's field. Qualitatively, this is achieved by utilizing the overshoot of the damped oscillation to tip the magnetization back into the x–y plane. We showed that this not only maximizes the ensuing free-precession signal, but also comes close to minimizing the duration of ringing that interferes with detection of the signal.

In the present paper we analyze the motion of **M** when the decay of B_p is *overdamped* and develop the condition for achieving adiabatic passage in minimum time. This method of rotating **M** to lie along the direction of the earth's field has been used by several research groups [3,4], who then used the traditional 90° pulse method to observe the magnetization at a later time. As an alternative to a 90° pulse, one could use a short "inspection pulse," whereby B_p is turned on adiabatically and then off suddenly, thereby leaving the magnetization precessing in the x–y plane [5]. This and other nonresonant methods of manipulating the direction of **M**, described here and in Refs. [1,2], are made possible by the fact that the coil field is easily made large compared to the earth's field B_e.

2. Overdamped cutoff

Fig. 1 is a schematic diagram of a typical circuit used to switch the polarizing current on and off in the earth's-field NMR experiment [6]. The circuit was discussed in [2] and is reproduced here for convenience. Capacitor C represents the stray capacitance of the coil and of the cable used to connect the coil to the remainder of the apparatus. In the present application resistance R will be chosen to produce adiabatic cutoff in minimum time.

With the electronic switch (Fig. 1) closed, polarizing current flows through the power supply, coil, and switch. At the end of the polarizing time the switch is opened; the voltage across the coil reverses and rises rapidly until the Zener diode begins to conduct, whereupon the coil current decays linearly toward zero. Near the end of cutoff the Zener stops conducting. At that instant the coil current is V_z/R and is decreasing at a rate V_z/L. These are the initial conditions for the subsequent damped oscillation. For typical coils, with the damping resistor adjusted to provide near-critical (or greater) damping, the coil current at the beginning of the transient will be sufficiently high to produce a coil field that is still several times larger than the earth's field. Thereafter, it is the details of the subsequent transient that control the motion of **M**.

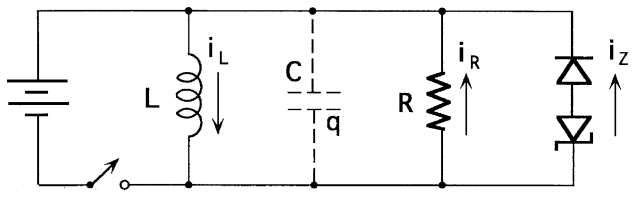

Fig. 1. Schematic diagram of a typical circuit used to switch the polarizing field on and off in an earth's-field NMR experiment.

In Appendix A it is shown that when the transient is highly overdamped, the field B_p is given approximately by

$$\frac{B_p}{B_e} = \rho_0 \Gamma e^{-\tau/\Gamma}. \tag{1}$$

Here, ω_e is the precession frequency in the earth's field, T is the decay time constant of the overdamped transient, and we have introduced the dimensionless quantities $\tau = \omega_e t$, $\Gamma = \omega_e T \approx 2\gamma/\omega_0^2$, $\omega_0 = (LC)^{-1/2}\omega_e^{-1}$, and $\gamma = (2RC\omega_e)^{-1}$. The quantity $\rho_0 \equiv |d(B_p/B_e)/d\tau|_0$ is a dimensionless constant that is a measure of the cutoff rate of B_p at $\tau = 0$ (see Eq. (A.2), Appendix A). Hence, the initial conditions at the beginning of the transient are

$$\left(\frac{B_p}{B_e}\right)_0 = \rho_0 \Gamma \tag{2a}$$

and

$$\frac{d}{d\tau}\left(\frac{B_p}{B_e}\right)_0 = -\rho_0. \tag{2b}$$

We now consider the case in which the motion of **M** is governed by an exponentially decaying transient, with $(B_p/B_e) \gg 1$ at time $\tau = 0$. Eq. (2a) indicates that this can be achieved by reducing R (thereby increasing Γ) or by increasing V_z (thereby increasing ρ_0), or some combination of the two, with the restriction that $\rho_0 \gg 1$ to ensure that sudden passage can also be obtained by switching to the appropriate value of R [2]. We are interested in the motion of **M** during exponential cutoff and in the conditions that must be met for adiabatic passage.

3. Numerical solution of the equations of motion

The equation of motion of the magnetization during the cutoff sequence is

$$\frac{d\mathbf{M}}{d\tau} = \mathbf{M} \times \left(\frac{\mathbf{B}}{B_e}\right), \tag{3}$$

where, as before, time t has been replaced by the dimensionless time parameter $\tau = \omega_e t$. We solve Eq. (3) subject to the assumption that the coil field B_p at the beginning of the transient, Eq. (2a), is at least 10 times the earth's field. It can then be assumed that the magnetization follows the resultant field **B** adiabatically during the linear portion of the cutoff ($\tau < 0$) and points in the direction of **B** at the beginning of the overdamped transient ($\tau = 0$).

Expanding the cross product in Eq. (3) and making the substitutions $B_x = 0$, $B_y = B_p$, and $B_z = B_e$ yields the coupled differential equations

$$\frac{dM_x}{d\tau} = M_y - \rho_0 \Gamma e^{-\tau/\Gamma} M_z, \tag{4a}$$

$$\frac{dM_y}{d\tau} = -M_x, \tag{4b}$$

$$\frac{dM_z}{d\tau} = \rho_0 \Gamma e^{-\tau/\Gamma} M_x. \tag{4c}$$

Eqs. (4a)–(4c) were solved numerically using the fourth-order Runge–Kutta algorithm. Since the magnitude of **M** is arbitrary, we fulfil the condition that **M** and **B** point in the same direction at time $\tau = 0$ by taking the initial conditions to be $M_x = 0$, $M_z = 1$, and $M_y = \rho_0 \Gamma$. Figs. 2a–c show, for $\rho_0 = 100$, the motion of the magnetization **M** for transients having time constants $\Gamma = 0.3$, $\Gamma = 0.6$, and $\Gamma = 1.2$. The solid line on the surface of each sphere shows the path traced out by the tip of the **M**-vector as the field $\mathbf{B}_p$ decays. The large value of ρ_0 is chosen so that the resultant field **B** and magnetization **M** both point essentially along the y-axis at $\tau = 0$ for a wide range of values of Γ. Little change occurs in the orientations of **B** and **M** until B_p drops to about five times B_e. At the instant when $B_p/B_e = 5$, and at six equally spaced time intervals (duration Γ) thereafter, the orientation of $\mathbf{B} = \mathbf{B}_p + \mathbf{B}_e$ is indicated by solid black circles along the arc in the y–z plane. The vectors in Figs. 2a–c show the orientation of **M** at the same instants of time. The paths in Fig. 2 follow the motion of **M** until the polarizing field B_p falls to less than 1% of the earth's field B_e, at which point the angle that **M** makes with the z-axis is within a few tenths of a degree of the final precession cone angle.

For B_p decays having short time constants, the motion of **M** is qualitatively similar to the case of linear cutoff

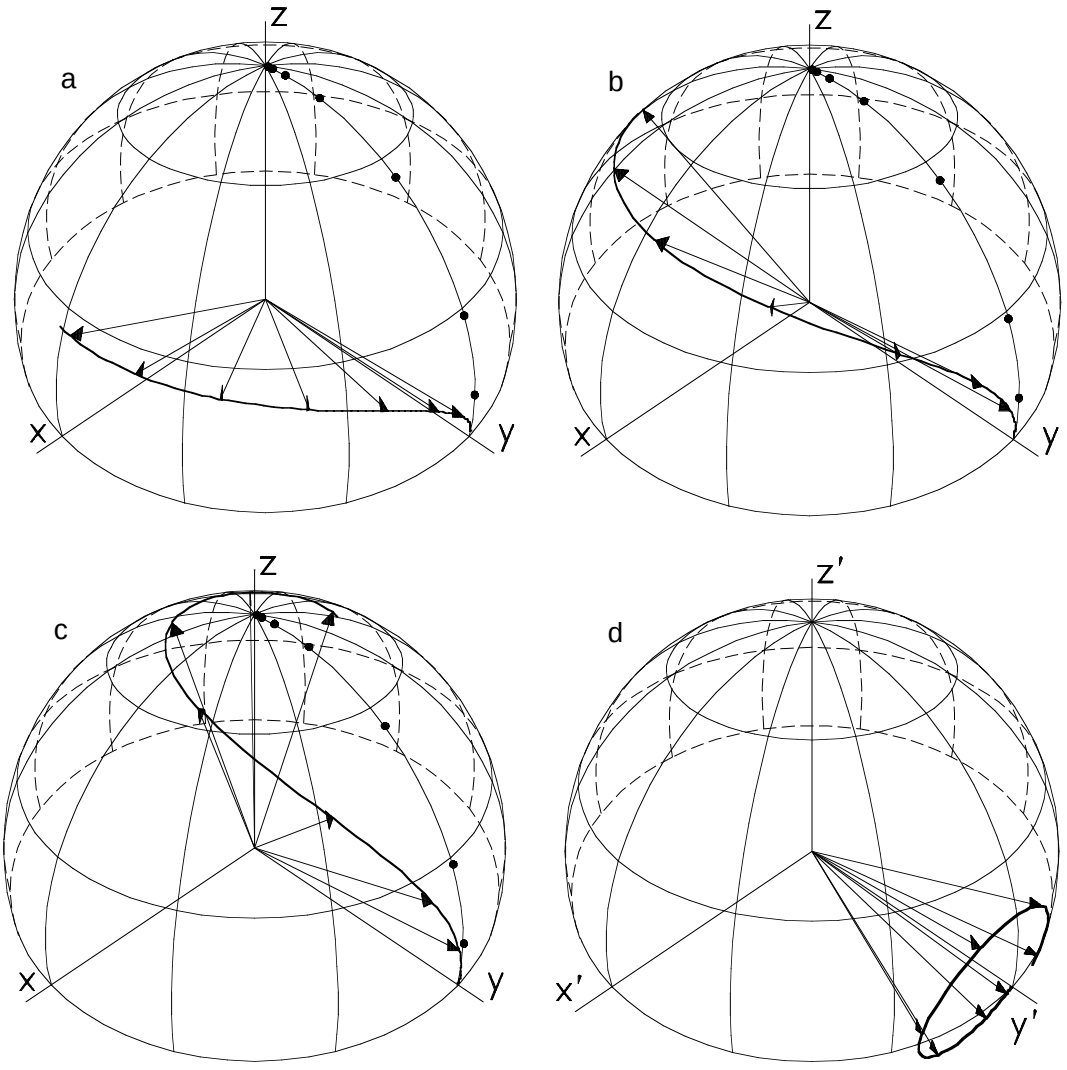

Fig. 2. Motion of magnetization **M** during cutoff for an initial cutoff rate $\rho_0 = 100$ and for three different time constants for the decay of the overdamped transient: (a) $\Gamma = 0.3$, (b) $\Gamma = 0.6$, (c) $\Gamma = 1.2$, (d) same as in (c), but shown from the point of view of an observer in the rotating frame (see Appendix B).

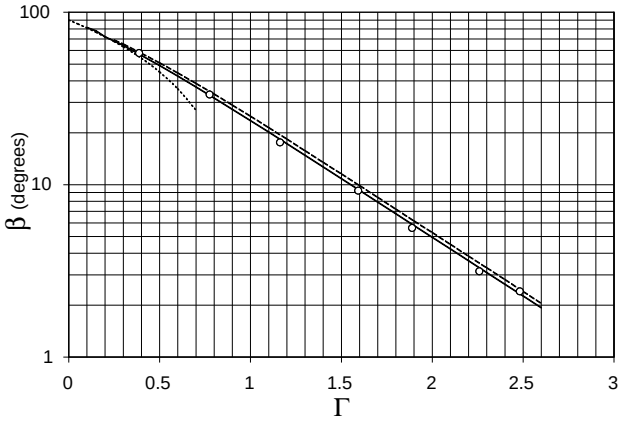

Fig. 3. Dependence of the free-precession cone angle on time constant of the decay of the overdamped switching transient. Values represented by the solid line were obtained from numerical solutions of Eqs. (4a)–(4c). Cone angles computed using the approximate Eq. (B.16) derived in Appendix B are denoted by the long dashed line. For both cases, calculations were made assuming $\rho_0 = 100$. The short dashed line shows cone angles computed using Eq. (6). The symbol ∘ indicates cone angles measured using the apparatus described in [6].

described in [1]. As the time constant increases, the magnetization follows **B** more and more closely and ends up precessing about $\mathbf{B}_e$ in a small cone of angle β. In Fig. 2c it is noteworthy that even though **M** does *not* follow **B** very closely, the passage is adiabatic from a practical point of view, in that the final cone angle β is small. In Fig. 3 we have plotted β, obtained from the numerical solutions, versus Γ. For decays having short time constants ($\Gamma \lesssim 0.4$) the cone angle decreases approximately linearly with Γ, while for slow decays ($\Gamma \gtrsim 1$) the cone angle decreases exponentially with Γ. The limiting forms, discussed further in Appendixes B and C, are

$$\beta = 2e^{-(\pi/2)\Gamma} \quad (\Gamma \gtrsim 1), \tag{5}$$

and

$$\beta = (1-\Gamma)\frac{\pi}{2} \quad (\Gamma \lesssim 0.4). \tag{6}$$

The fact that $\beta(\Gamma)$ has these simple limiting forms suggests that closed-form solutions may be possible. In Appendix B we attempt a solution for the adiabatic limit, and in Appendix C for the sudden passage limit. The results are shown as dashed curves in Fig. 3. For the sudden passage limit we were able to derive Eq. (6), but the solution for the adiabatic limit led to simultaneous differential equations, one of which contained a small nonlinear term. Neglecting this term leads to the corresponding dashed curve in Fig. 3.

4. Experimental results

The apparatus described in [6] was used to perform an experimental test of these results. Damping resistor R (Fig. 1) was varied, and for each value of resistance the decay time constant of the overdamped transient and the amplitude (V) of the ensuing free-precession signal were measured. The final precession cone angle was then calculated from $\beta = \sin^{-1}(V/V_{max})$, where V_{max} is the signal amplitude obtained from sudden passage, as described in [2]. For large damping, the coil current decays were exponential. Near critical damping, where the overdamped decays were noticeably nonexponential, we measured the time constants at the ends of the decay—i.e., after the short time constant component had become negligibly small. The experimental results are shown in Fig. 3. The agreement between the predicted and measured results is very good, especially considering the difficulty of aligning the coil axis to make it exactly perpendicular to the earth's magnetic field. Such alignment is critical: numerical solutions of the equations of motion show that, for slow cutoffs near $\Gamma = 2.5$, varying the angle between the coil axis and the earth's field between 89° and 91° results in a variation of about 0.4°, or ±8%, in the cone angle of the ensuing free precession.

5. Discussion

The details of the motion of **M** depend on the time dependence of $\mathbf{B}_p$ and on the initial conditions. Exceedingly complex motions are possible, even for relatively simple physical situations, such as a **B**-field of constant magnitude rotating at constant angular velocity.

For the numerical integration, it is necessary that the successive time increments used be short compared to the instantaneous precession period. This comes about because the changes in the instantaneous precession cone angle depend on whether the **M**-vector happens to be ahead of, behind, or to the side of the rotating **B**-vector. In the problem at hand, this results in a kind of "Zitterbewegung"—tiny oscillations of **M** at frequencies near the instantaneous precession frequency. Although these oscillations are much too small to show up in Figs. 2a–c, they are, in fact, involved in determining the rate at which the precession cone angle changes in time. Mathematically, this manifests itself in the complicated integrand in Eq. (B.16) (Appendix B), which oscillates at these high and variable frequencies in certain ranges of the variable of integration. Thus the "area under the curve" also oscillates rapidly, but accumulates only slowly in these regions.

Sudden and adiabatic passage occur, respectively, when $d\alpha/dt$ is large or small compared to the precession frequency ω at the instant in question. The initial part of the motion of **M** is always adiabatic, and for exponential decay of B_p the final part is adiabatic as well. The final cone angle depends on the degree of "nonadiabaticity" *throughout* the passage. A good measure of "nonadi-

abaticity" is the ratio of $d\alpha/dt$ and ω, or, in dimensionless units, the ratio $(d\alpha/d\tau)/(\omega/\omega_e)$. It is readily shown that $d\alpha/d\tau = -(2\Gamma)^{-1}\sin 2\alpha$ (see Appendix B) and $(d\alpha/d\tau)/(\omega/\omega_e) = -(\Gamma)^{-1}\sin\alpha\cos^2\alpha$, so that if $\Gamma \gtrsim 1$ the motion of **M** is adiabatic *throughout* the passage. Also, the maximum $d\alpha/d\tau$ occurs when $\alpha = 45°$, and the maximum $(d\alpha/d\tau)/(\omega/\omega_e)$ occurs when $\alpha = \sin^{-1}(1/\sqrt{3}) \approx 35°$. The latter is also the value of α at which the resultant field in the rotating frame (Appendix B) is tilted furthest from the y'-axis. A characteristic of the motion of **M** is that the instantaneous cone angle (angle between **M** and **B**) passes through a maximum before settling down to its final value β.

For a typical earth's-field NMR instrument, it is the details of the switching transient at the end of rapid cutoff of the polarizing field that ultimately determine whether the cutoff is sudden or adiabatic. Either may be achieved by a suitable choice of damping resistor in parallel with the coil. As the damping resistance is gradually reduced, the transition from sudden to adiabatic passage occurs over a sufficiently broad range so that practically any desired final free-precession cone angle can readily be obtained. As can be seen from the results in Fig. 3, near-perfect adiabatic passage (magnetization aligned within 2° of the earth's field) can be achieved for time constants $T \geqslant 2.6/\omega_e$. For a typical precession frequency of 2.1 kHz, $T = 2.6/\omega_e$ corresponds to a time constant of about 0.2 ms. For $\rho_0 = 100$, about 10 time constants are required for B_p to decay to $0.01B_e$, so that the adiabatic cutoff takes about 2 ms. This is short compared to the shortest relaxation times ($T_2 \sim 20$ ms) that can be measured with the earth's-field technique.

Appendix A

Fig. 1 shows the essential elements of the circuit that determines the time dependence of the decay of the coil current after the Zener diode stops conducting. Here, R is an equivalent parallel resistance that includes all resistive losses, and C represents the stray capacitance of the coil, connecting cable, etc. Since the coil is high-Q, the resistance R is essentially the same as that of the physical resistor used to produce overdamping.

The circuit functions as previously described. While the Zener diode is conducting, the polarizing field along the axis of the coil decreases at a constant rate

$$\frac{dB_p}{dt} = -\frac{(B/I)V_z}{L}, \tag{A.1}$$

where (B/I) is the field-to-current ratio for the coil. By introducing the dimensionless time parameter $\tau = \omega_e t$, where ω_e represents the proton precession frequency in the earth's field B_e, the linear cutoff rate of the polarizing field, in dimensionless units, can be written in the form

$$\rho_0 \equiv \left|\frac{d}{d\tau}\left(\frac{B_p}{B_e}\right)_0\right| = \frac{(B/I)V_z}{L\omega_e B_e}. \tag{A.2}$$

Capacitor C, which is charged to the Zener voltage V_z during the linear portion of the cutoff, prevents the cutoff rate from changing instantaneously when the Zener diode stops conducting at time $t = 0$. Therefore, ρ_0 also represents the initial cutoff rate at the beginning of the overdamped transient at $t = 0$.

For $t \geqslant 0$ the coil current is given by the solution to the differential equation [8]

$$\frac{d^2 i_L}{dt^2} + \frac{1}{RC}\frac{di_L}{dt} + \frac{1}{LC}i_L = 0. \tag{A.3}$$

The solution to Eq. (A.3) for the overdamped case, subject to the initial conditions $i_L = i_0 = V_z/R$ and $di_L/dt = -V_z/L$, is

$$i_L = \frac{i_0}{\gamma_+ - \gamma_-}\left[\left(\gamma_+ - \frac{\omega_0^2}{2\gamma}\right)e^{-\gamma_-\tau} - \left(\gamma_- - \frac{\omega_0^2}{2\gamma}\right)e^{-\gamma_+\tau}\right]. \tag{A.4}$$

In Eq. (A.4) we have introduced the dimensionless parameters $\gamma = (2RC\omega_e)^{-1}$, $\omega_0 = (LC)^{-1/2}\omega_e^{-1}$, $\gamma_+ = \gamma + (\gamma^2 - \omega_0^2)^{1/2}$, and $\gamma_- = \gamma - (\gamma^2 - \omega_0^2)^{1/2}$. The field B_p that this current produces, as a multiple of the earth's field, is

$$\frac{B_p}{B_e} = \frac{(B/I)i_L}{B_e} = \frac{2\gamma\rho_0}{\omega_0^2(\gamma_+ - \gamma_-)}\left[\left(\gamma_+ - \frac{\omega_0^2}{2\gamma}\right)e^{-\gamma_-\tau} - \left(\gamma_- - \frac{\omega_0^2}{2\gamma}\right)e^{-\gamma_+\tau}\right]. \tag{A.5}$$

For small damping, with γ only slightly greater than ω_0, we have $\gamma_+ \approx \gamma_-$, and the two terms inside the brackets in Eq. (A.5) have approximately the same amplitude and decay at about the same rate. For large damping, such that $\omega_0^2/\gamma^2 \ll 1$, we make the approximations $\gamma_+ \approx 2\gamma$ and $\gamma_- \approx \omega_0^2/2\gamma$. Eq. (A.5) then simplifies to

$$\frac{B_p}{B_e} = \rho_0\Gamma e^{-\tau/\Gamma}, \tag{A.6}$$

where the time constant for the exponential decay, in dimensionless units, is $\Gamma = 1/\gamma_- \approx 2\gamma/\omega_0^2$. The time constant in seconds is $T = \Gamma/\omega_e$.

To verify the validity of the above approximation, we obtained the equations of motion of **M** using, in place of Eq. (A.6), the more exact Eq. (A.5), thus taking into account the fact that the overdamped transient is actually the difference of two terms that decay at different rates. We chose $\rho_0 = 32.2$ and $\omega_0 = 3.86$, which are the measured parameters for the earth's-field NMR apparatus described in [6], and solved the equations numerically for various assumed values of the damping constant γ. A graph of the cone angles β obtained from these solutions, plotted versus the dimensionless time constant

$\Gamma = 1/\gamma_-$, was found to be virtually indistinguishable from the solid-line graph in Fig. 3. Thus, the simplifying assumption of a pure exponential decay is well justified in practice, and the value assumed for ρ_0 is not critical as long as the condition $(B_p/B_e)_0 \gg 1$ is satisfied.

Appendix B

We seek solutions to Eqs. (4a)–(4c), valid for slow cutoffs, for which the magnetization follows **B** nearly adiabatically and ends up precessing about the earth's field in a small cone having cone angle β. Since the magnitude of **M** is constant, transforming to spherical coordinates leads to two coupled differential equations in the spherical angles θ and φ. However, these equations are tractable only in the small-angle approximation, and this approximation must remain valid throughout the passage. This suggests seeking solutions in a rotating frame that follows the resultant field $\mathbf{B} = \mathbf{B}_p + \mathbf{B}_e$. This rotating (primed) frame is shown in Fig. 4. The y'-axis is chosen to be along the resultant field, and it rotates about the x–x' axis, starting initially in very nearly the same direction as the polarizing field $\mathbf{B}_p$. As $\mathbf{B}_p$ decays toward zero, the y'-axis approaches its final orientation along the z-axis, which is in the direction of the earth's field $\mathbf{B}_e$. The magnitude of the angular velocity of rotation is $|d\alpha/dt|$, where α (Fig. 4) is the polar angle between the resultant field **B** and the earth's field $\mathbf{B}_e$. In the rotating frame, in addition to the resultant field **B** along the y'-axis, there is a fictitious field along the $+x'$-axis given, in dimensionless units, by

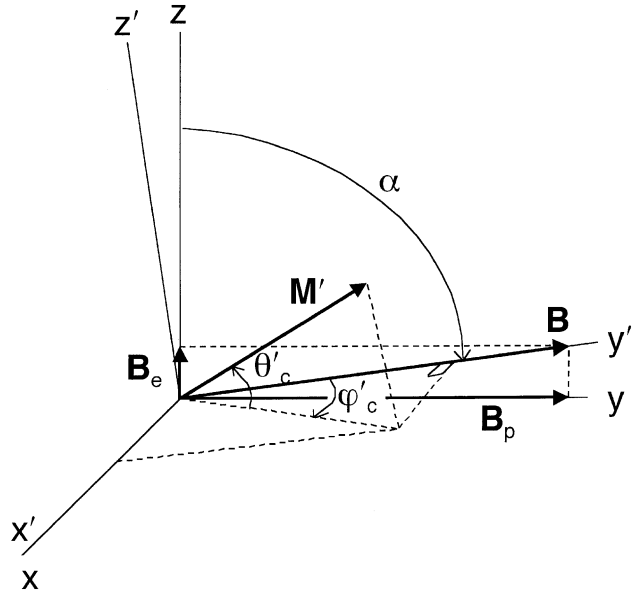

Fig. 4. Rotating frame of reference with the y'-axis directed along the resultant field $\mathbf{B} = \mathbf{B}_p + \mathbf{B}_e$. As the transient decays and the polarizing field shrinks from $B_p \gg B_e$ to $B_p \approx 0$, the primed frame rotates through approximately 90°.

$$\frac{\mathbf{B}_f}{B_e} = \mathbf{i}'\left|\frac{d\alpha}{d\tau}\right|, \tag{B.1}$$

where, as before, we have made the substitution $\tau = \omega_e t$. As viewed in the rotating frame, the magnetization $\mathbf{M}'$ tends to precess about the vector sum of **B** and $\mathbf{B}_f$, which is the resultant field in the rotating frame. In the adiabatic limit $d\alpha/d\tau$ is small, so that $\mathbf{M}'$ never strays far from the y'-axis. Hence, in the primed frame, the *complements* of the spherical angles θ' and φ' will be small throughout adiabatic passage.

Using Eqs. (1) and (B.1), and noting from Fig. 4 that $\tan\alpha = B_p/B_e$, we obtain

$$\frac{\mathbf{B}_f}{B_e} = \frac{\mathbf{i}'}{2\Gamma}\sin 2\alpha. \tag{B.2}$$

Near the beginning and end of the overdamped transient, where α approaches 90° and 0°, respectively, the fictitious field $\mathbf{B}_f$ approaches zero. Near those extremes, the angular velocity of the rotating frame is very small. The fictitious field is a maximum when $\alpha = 45°$, which occurs at the instant when $B_p = B_e$.

The equation of motion in the rotating frame

$$\frac{d\mathbf{M}'}{d\tau} = \mathbf{M}' \times \left(\frac{\mathbf{B}}{B_e} + \frac{\mathbf{B}_f}{B_e}\right) \tag{B.3}$$

is somewhat easier to solve if, instead of finding $\mathbf{M}'$ as a function of time, we seek instead solutions for $\mathbf{M}'$ as a function of α. By using Eqs. (1) and (B.2), and noting from Fig. 4 that $B/B_e = \sec\alpha$, we obtain by straightforward substitution into Eq. (B.3) the equations of motion

$$\frac{dM'_x}{d\alpha} = \frac{2\Gamma}{\sin 2\alpha\cos\alpha}M'_z, \tag{B.4a}$$

$$\frac{dM'_y}{d\alpha} = -M'_z, \tag{B.4b}$$

$$\frac{dM'_z}{d\alpha} = \frac{-2\Gamma}{\sin 2\alpha\cos\alpha}M'_x + M'_y. \tag{B.4c}$$

Following a procedure similar to that used in [1,2], we solve Eqs. (B.4a)–(B.4c) by changing variables and expressing M'_x, M'_y, and M'_z in terms of θ'_c and φ'_c, the complements of the spherical polar angles θ' and φ' in the rotating frame (see Fig. 4). We obtain

$$\frac{d\theta'_c}{d\alpha} = \cos\varphi'_c - \frac{2\Gamma}{\sin 2\alpha\cos\alpha}\sin\varphi'_c \tag{B.5}$$

and

$$\frac{d\varphi'_c}{d\alpha} = \frac{2\Gamma}{\sin 2\alpha\cos\alpha}\tan\theta'_c\cos\varphi'_c + \tan\theta'_c\sin\varphi'_c. \tag{B.6}$$

Linearizing Eqs. (B.5) and (B.6) about $\theta'_c = 0$ and $\varphi'_c = 0$ gives the system

$$\frac{d\theta'_c}{d\alpha} = 1 - \varphi'_c\frac{d\xi}{d\alpha} \tag{B.7}$$

and

$$\frac{d\varphi_c'}{d\alpha} = \theta_c' \frac{d\xi}{d\alpha} + \theta_c' \varphi_c', \tag{B.8}$$

where the function ξ is defined by

$$\xi(\alpha) = \Gamma\left(\sec\alpha + \ln\tan\frac{\alpha}{2}\right). \tag{B.9}$$

If we neglect the product $\theta_c'\varphi_c'$ in Eq. (B.8), Eqs. (B.7) and (B.8) can be solved by introducing a complex function f defined by $f = \theta_c' + i\varphi_c'$ and by showing that f is a solution to

$$\frac{df}{d\alpha} = 1 + if\frac{d\xi}{d\alpha}. \tag{B.10}$$

A general solution for f is

$$\theta_c' + i\varphi_c' = e^{i\xi(\alpha)} \int_{\alpha_0}^{\alpha} e^{-i\xi(s)}\, ds + ce^{i\xi(\alpha)}, \tag{B.11}$$

where $\alpha_0 = \tan^{-1}[(B_p/B_e)_0] = \tan^{-1}[\rho_0\Gamma] \approx \pi/2$, and c is a constant of integration. Assuming $\mathbf{M}'$ points along the y'-axis in the direction of $\mathbf{B}$ at time $t = 0$, we require $c = 0$. Equating the real and imaginary parts of Eq. (B.11) gives the solutions

$$\theta_c'(\alpha) = \cos\xi(\alpha) \int_{\alpha_0}^{\alpha} \cos\xi(s)\, ds + \sin\xi(\alpha) \int_{\alpha_0}^{\alpha} \sin\xi(s)\, ds \tag{B.12}$$

and

$$\varphi_c'(\alpha) = \sin\xi(\alpha) \int_{\alpha_0}^{\alpha} \cos\xi(s)\, ds - \cos\xi(\alpha) \int_{\alpha_0}^{\alpha} \sin\xi(s)\, ds. \tag{B.13}$$

Near the end of the transient, the polarizing field and angle α shrink toward zero. For small angles, $\xi(\alpha)$ can be approximated by $\Gamma[1 + \ln(\alpha/2)]$, and α approaches $B_p/B_e = \rho_0\Gamma e^{-\tau/\Gamma}$. Furthermore, numerical integration shows that, for $\alpha \approx 0$, the cosine integrals in Eqs. (B.12) and (B.13) are large compared to the sine integrals. Neglecting the latter, we obtain

$$\theta_c'(\tau) \approx \left(\int_{\alpha_0}^{0} \cos\xi(s)\, ds\right) \cos\left[\Gamma\left(1 + \ln\frac{\rho_0\Gamma}{2}\right) - \tau\right] \tag{B.14}$$

and

$$\varphi_c'(\tau) \approx \left(\int_{\alpha_0}^{0} \cos\xi(s)\, ds\right) \sin\left[\Gamma\left(1 + \ln\frac{\rho_0\Gamma}{2}\right) - \tau\right]. \tag{B.15}$$

Eqs. (B.14) and (B.15) apply after the transient has essentially decayed to zero and describe a precession of magnetization $\mathbf{M}'$ at frequency $\omega/\omega_e = 1$, with cone angle β given by

$$\beta = \left|\int_{\alpha_0}^{0} \cos\xi(s)\, ds\right| \approx \left|\int_{\pi/2}^{0} \cos\xi(s)\, ds\right| = \left|\int_{\pi/2}^{0} \cos\left[\Gamma\left(\sec s + \ln\tan\frac{s}{2}\right)\right] ds\right|. \tag{B.16}$$

Here, $\alpha_0 = \tan^{-1}[\rho_0\Gamma] \approx \pi/2$. Eq. (B.16) was evaluated numerically using Mathematica. The results for $\rho_0 = 100$ are plotted in Fig. 3 as a long dashed curve. The agreement with the Runge–Kutta solution in the fixed frame is surprisingly good over the whole range of values of Γ investigated, even for Γ-values that correspond to final cone angles greater than 30°, for which the small-angle approximations are clearly not justified.

Inspection of Fig. 3 shows that there *is* a small systematic discrepancy between the cone angles computed from Runge–Kutta in the fixed frame and those calculated using the small-angle approximation in the rotating frame. The discrepancy persists even for $\Gamma > 2$, for which the small-angle approximations should be very good. The discrepancy is due to neglecting the product term $\theta_c'\varphi_c'$ in Eq. (B.8). When this term is retained and Eqs. (B.7) and (B.8) are solved numerically, the results for slow decays ($\Gamma \geqslant 2$) agree almost exactly with the results obtained from the numerical solution in the fixed frame.

Appendix C

We seek solutions to Eqs. (4a)–(4c), valid for *rapid* cutoffs, for which the magnetization remains close to the x–y plane. Following a procedure similar to that in Appendix B, we express M_x, M_y, and M_z in terms of θ_c and φ_c, the complements of the spherical polar angles θ and φ in the fixed frame. After linearizing the equations about $\theta_c = 0$ and $\varphi_c = 0$ we obtain

$$\frac{d\theta_c}{d\tau} = \varphi_c \frac{d\varsigma}{d\tau} \tag{C.1}$$

and

$$\frac{d\varphi_c}{d\tau} = 1 - \theta_c \frac{d\varsigma}{d\tau}, \tag{C.2}$$

where the function ζ is defined by

$$\zeta(\tau) = -\rho_0\Gamma^2 e^{-\tau/\Gamma}. \tag{C.3}$$

Eqs. (C.1) and (C.2) can be solved by introducing a complex function f defined by $f = \varphi_c + i\theta_c$ and by showing that f is a solution to

$$\frac{df}{d\tau} = 1 + if\frac{d\varsigma}{d\tau}. \tag{C.4}$$

A general solution to Eq. (C.4) is

$$\varphi_c + i\theta_c = e^{i\zeta(\tau)} \int_0^{\tau} e^{-i\zeta(s)}\, ds + ce^{i\zeta(\tau)}, \tag{C.5}$$

where c is a constant of integration. Assuming the magnetization points in the direction of the resultant field **B** at time $\tau = 0$, we obtain, using Eq. (2a),

$$c = \frac{\mathrm{i}}{\rho_0 \Gamma} \mathrm{e}^{-\mathrm{i}\zeta(0)}. \tag{C.6}$$

Substituting Eq. (C.6) into Eq. (C.5) and equating the real and imaginary parts gives the solutions

$$\theta_c(\tau) = S(\tau) \int_0^\tau C(s)\,\mathrm{d}s - C(\tau) \int_0^\tau S(s)\,\mathrm{d}s + \frac{1}{\rho_0 \Gamma}[C(0)C(\tau) + S(0)S(\tau)] \tag{C.7}$$

and

$$\varphi_c(\tau) = S(\tau) \int_0^\tau S(s)\,\mathrm{d}s + C(\tau) \int_0^\tau C(s)\,\mathrm{d}s + \frac{1}{\rho_0 \Gamma}[S(0)C(\tau) - C(0)S(\tau)], \tag{C.8}$$

where we have made the substitutions

$$C(\tau) = \cos\zeta(\tau) \tag{C.9}$$

and

$$S(\tau) = \sin\zeta(\tau). \tag{C.10}$$

For the case analyzed in this paper $1/\rho_0 \Gamma \ll 1$. Therefore, the last terms in Eqs. (C.7) and (C.8) make only small contributions to the computed values of θ_c and φ_c. For large τ, such that $\tau \gg \Gamma$, we make the approximations $C(\tau) \approx C(\infty) = 1$, and $S(\tau) \approx S(\infty) = 0$. Neglecting the small contribution from the last term, we obtain from Eq. (C.7) the approximate result

$$\theta_c(\infty) \approx -\int_0^\infty S(s)\,\mathrm{d}s = \int_\infty^0 \sin\zeta(s)\,\mathrm{d}s. \tag{C.11}$$

Using Eq. (C.3), and changing variables by making the substitution $u = \zeta(s)$, Eq. (C.11) can be written

$$\theta_c(\infty) \approx \Gamma \mathrm{Si}(\rho_0 \Gamma^2), \tag{C.12}$$

where Si is the sine integral function

$$\mathrm{Si}(x) = \int_0^x \frac{\sin u}{u}\,\mathrm{d}u. \tag{C.13}$$

For large values of $\rho_0 \Gamma^2$, $\mathrm{Si}(\rho_0 \Gamma^2)$ approaches $\pi/2$ [7]. Hence, the final cone angle of the free precession is given by

$$\beta = \frac{\pi}{2} - \theta_c(\infty) \approx (1 - \Gamma)\frac{\pi}{2}. \tag{C.14}$$

For rapid exponential decays that leave the magnetization near the x–y plane (sudden passage) the final cone angle decreases linearly with time constant.

References

[1] B.F. Melton, V.L. Pollak, T.W. Mayes, B.L. Willis, Condition for sudden passage in the earth's-field NMR technique, J. Magn. Reson. A 117 (1995) 164–170.
[2] B.F. Melton, V.L. Pollak, Optimizing sudden passage in the earth's-field NMR technique, J. Magn. Reson. A 122 (1996) 42–49.
[3] J. Stepišnik, V. Eržen, M. Kos, NMR imaging in the earth's magnetic field, Magn. Reson. Med. 15 (1990) 386–391.
[4] P.T. Callaghan, C.D. Eccles, J.D. Seymour, An earth's field nuclear magnetic resonance apparatus suitable for pulsed gradient spin echo measurements of self-diffusion under Antarctic conditions, Rev. Sci. Instrum. 68 (1997) 4263–4270.
[5] B.F. Melton, Proton spin relaxation in liquid $CHCl_3$ and in H_2O–D_2O solutions of chromium(III), PhD Thesis, Oklahoma State University, 1970.
[6] B.F. Melton, V.L. Pollak, Instrumentation for the earth's field NMR technique, Rev. Sci. Instrum. 42 (1971) 769–773.
[7] M. Abramowitz, I.A. Stegun (Eds.), Handbook of Mathematical Functions with Formulas, Graphs, and Mathematical Tables, US Government Printing Office, Washington, DC, 1964, p. 232.
[8] A discussion of damped parallel resonant LC circuits may be found in many textbooks dealing with linear circuit analysis. See, for example L.S. Bobrow, in: Elementary Linear Circuit Analysis, second ed., Oxford University Press, New York, 1987, p. 280.